Cellular/Molecular

Regulation of Kv2.1 K^+ Conductance by Cell Surface Channel Density

Philip D. Fox,[1] Rob J. Loftus,[1] and Michael M. Tamkun[1,2]

[1]Department of Biomedical Sciences and [2]Department of Biochemistry and Molecular Biology, Colorado State University, Fort Collins, Colorado 80523

The Kv2.1 voltage-gated K^+ channel is found both freely diffusing over the plasma membrane and concentrated in micron-sized clusters localized to the soma, proximal dendrites, and axon initial segment of hippocampal neurons. In transfected HEK cells, Kv2.1 channels within cluster microdomains are nonconducting. Using total internal reflection fluorescence microscopy, the number of GFP-tagged Kv2.1 channels on the HEK cell surface was compared with K^+ channel conductance measured by whole-cell voltage clamp of the same cell. This approach indicated that, as channel density increases, nonclustered channels cease conducting. At the highest density observed, only 4% of all channels were conducting. Mutant Kv2.1 channels that fail to cluster also possessed the nonconducting state with 17% conducting K^+ at higher surface densities. The nonconducting state was specific to Kv2.1 as Kv1.4 was always conducting regardless of the cell-surface expression level. Anti-Kv2.1 immunofluorescence intensity, standardized to Kv2.1 surface density in transfected HEK cells, was used to determine the expression levels of endogenous Kv2.1 in cultured rat hippocampal neurons. Endogenous Kv2.1 levels were compared with the number of conducting channels determined by whole-cell voltage clamp. Only 13 and 27% of the endogenous Kv2.1 was conducting in neurons cultured for 14 and 20 d, respectively. Together, these data indicate that the nonconducting state depends primarily on surface density as opposed to cluster location and that this nonconducting state also exists for native Kv2.1 found in cultured hippocampal neurons. This excess of Kv2.1 protein relative to K^+ conductance further supports a nonconducting role for Kv2.1 in excitable tissues.

Introduction

Voltage-gated K^+ channels (Kv) are expressed in most excitable cells where they regulate membrane potential. Kv2.1 is among the most ubiquitously expressed Kv channel subunits in the mammalian brain where it mediates the majority of the delayed rectifier current (Ik_{DR}) in principal neurons of the hippocampus and cortex and regulates the action potential waveform during repetitive stimulation (Murakoshi and Trimmer, 1999; Du et al., 2000; Malin and Nerbonne, 2002; Guan et al., 2007). Unique to Kv2.1 is its localization to high-density cell-surface clusters in intact brain, cultured neurons, and transfected HEK cells (Lim et al., 2000; Misonou et al., 2005; O'Connell and Tamkun, 2005). In addition, there is a second population of nonclustered Kv2.1 channels, which are spread diffusely over the cell surface (O'Connell et al., 2006). Kv2.1 clusters are dynamic structures that disperse and release channels in response to noxious stimuli, such as ischemia, hypoxia, and glutamate excitotoxicity (Misonou et al., 2008; Mulholland et al., 2008). Associated with the release of Kv2.1 from clusters is a leftward shift in activation midpoint, likely induced by dephosphorylation within the intracellular C-terminus (Misonou et al., 2004; Park et al., 2006). It was postulated that channels residing within clusters have a high threshold for activation, whereas nonclustered channels have a lower activation threshold.

Recently, we discovered using cell-attached patch-clamp that channels residing within clusters are almost exclusively held in a nonconducting state, contradicting the hypothesis that clustered Kv2.1 are high-threshold channels with respect to their voltage sensitivity (O'Connell et al., 2010). However, cell-attached patch-clamp recordings can underestimate the number of voltage-gated sodium channels in the axon initial segment resulting from interference of the actin cytoskeleton (Kole et al., 2008), raising the possibility that the nonconducting Kv2.1 was an artifact of the cell-attached patch-clamp technique. In addition, it was possible that the nonconducting state is specific to Kv2.1 channels expressed in HEK cells and does not apply to the endogenous channel in hippocampal neurons, even though the neuronal machinery affecting Kv2.1 localization and function is present in HEK cells (Mohapatra and Trimmer, 2006), which is perhaps not surprising because HEK cells express many neuronal markers and may be of neuronal origin (Shaw et al., 2002).

To address the first issue, we performed whole-cell voltage clamp recordings on HEK cells in conjunction with internal reflection fluorescence (TIRF)-based quantitation of cell-surface Kv2.1 channel density to relate channel number to channel conductance. This approach also identified a large nonconducting population of channels. The second issue was addressed by standardizing anti-Kv2.1 immunolabeling to Kv2.1 surface density in

Received June 25, 2012; revised Nov. 30, 2012; accepted Dec. 2, 2012.

Author contributions: P.D.F. and M.M.T. designed research; P.D.F. and R.J.L. performed research; P.D.F. and M.M.T. analyzed data; P.D.F. and M.M.T. wrote the paper.

This work was supported by the National Institutes of Health Grants R01GM84136 and R01GM084136S1 to M.M.T. We thank Jozeph Vigh, Aubrey Wiegel, and Elizabeth Akin for critical review of the manuscript.

The authors declare no competing financial interests.

Correspondence should be addressed to Dr. Michael M. Tamkun, Department of Biomedical Sciences, 1617 Campus Delivery, Colorado State University, Ft. Collins, CO 80523-1617. E-mail: michael.tamkun@colostate.edu.

DOI:10.1523/JNEUROSCI.3008-12.2013

Copyright © 2013 the authors 0270-6474/13/331259-12$15.00/0

the HEK cell system and then determining the expression levels of the endogenous Kv2.1 in cultured hippocampal neurons via immunofluorescence. We find that the nonconducting state depends more on surface density than on location within a cluster and that this nonconducting state also exists for the native Kv2.1 found in cultured hippocampal neurons.

Materials and Methods

Plasmid constructs, cell culture, and transfections. Fluorescent protein tagged Kv channel constructs, based on the Living Colors vector system (Clontech), have been described previously (Scannevin et al., 1996; O'Connell and Tamkun, 2005; O'Connell et al., 2006; Tamkun et al., 2007). The N-terminal fusion of Kv1.4 with GFP blocks the fast inactivation normally seen with this channel (Tseng-Crank et al., 1993). HEK 293 cells (American Type Culture Collection, passage 38–45) cells were transfected with 0.5–3 μg of Kv-expressing DNA using a Bio-Rad Genepulser Xcell (Bio-Rad) with a 0.2-cm-gap cuvette and a single 110 V 25 ms pulse. Transfected cells were then plated on glass-bottom 35 mm dishes (Mattek) that had been coated previously with Matrigel (BD Biosciences) and covered in DMEM + 10% FBS. HEK cells were imaged within 24 h of electroporation in HEK physiological saline consisting of (in mM): 146 NaCl, 4.7 KCl, 2.5 $CaCl_2$, 1 $MgCl_2$, 10 glucose, and 10 HEPES, pH 7.4. Neurons from cryo-preserved E18 rat hippocampal dissociations of both sexes were plated at a density of ~15,000–30,000 cells/cm^2 on poly-D-lysine-coated glass-bottom dishes (Mattek) and cultured in glial-cell conditioned neurobasal medium containing B27 supplement (Invitrogen) as previously described (O'Connell et al., 2006). Every 3–4 d after plating, one-half of the culture medium was replaced with glial-cell conditioned neurobasal medium. Animals were deeply anesthetized with isoflurane and euthanized by decapitation according to a protocol approved by the Institutional Animal Care and Use Committee of Colorado State University.

Immunocytochemistry. Neurons and HEK cells were fixed with 4% formaldehyde, in PBS for 15 min at 37°C, incubated in 0.5% CHAPS in PBS, blocked in 10% goat serum in PBS, and labeled with the indicated antibody diluted in PBS containing 1% BSA. A mouse monoclonal anti-Kv2.1 antibody (NeuroMabs, 1:1000 dilution) was used in conjunction with a goat anti-mouse secondary antibody conjugated to Alexa Fluor 594 (Invitrogen), diluted 1:1000 in 1% BSA PBS (Misonou et al., 2005). For live-cell labeling, HEK cells expressing GFP-Kv2.1-HA were labeled for 15 min at 37°C with a 1:1000 dilution of an anti-HA antibody conjugated to Alexa Fluor-594 (Invitrogen) in physiological saline containing 1% BSA.

3D quantification of clustered membrane area. HEK cells transfected with GFP-Kv2.1 were labeled with DiI at 37°C for 5 min and washed 3× with imaging saline before imaging. Cultured hippocampal neurons were labeled with FITC-conjugated wheat germ agglutinin (WGA) at 37°C for 5 min and washed 3× with imaging saline before fixation and subsequent immunolabeling for endogenous Kv2.1. Confocal *z*-steps (0.3 μm) were acquired for 3D reconstruction, and the intensities of all fluorophores were adjusted so that the fluorescent volume would be similar and could be used as a relative measure of surface area. Either Kv2.1 clusters or the entire membrane was measured in 3D using an automated object finding protocol in Volocity Version 6.0 (PerkinElmer). Occasionally, intracellular fluorescence was aberrantly selected by the object finding protocol. To avoid this potential artifact, intracellular fluorescence was removed in Adobe Photoshop to within 1 μm of the PM as determined by the DiI or WGA. In neurons, this analysis was restricted to the soma and the most proximal portions of the neurites where Kv2.1 clusters typically form.

Measurement of single-channel GFP intensity. HEK cells transfected with GFP-Kv2.1 were photobleached during TIRF imaging, and single GFP molecule fluorescence intensity was determined by quantitating the bleach-step magnitude. The fluorescence intensity of a single channel was divided by the mean bleach-step magnitude and the data placed into bins of 0.5–1.5, 1.5–2.5, 2.5–3.5, and 3.5–4.5. Any puncta >4.5-fold the mean single GFP bleach-step magnitude were excluded from the analysis because these could represent multiple channels. The binned data were fit to a binomial distribution of four fluorescent GFP molecules with an independent folding efficiency for GFP of 74% (see Fig. 2*C*) (Sugiyama et al., 2005; Ulbrich and Isacoff, 2007; Plant et al., 2011).

In the electrophysiology experiments, it was impractical to obtain individual bleach steps because the majority of cell recordings were discarded for voltage-clamp quality control issues, increasing series resistance, increasing membrane leak, etc. Instead, the fluorescent intensity of discrete puncta from a nearby cell was measured from a single frame where the intensity was greatest. The brightest puncta correspond to single channels with four functional GFP molecules. These measurements were divided by four and averaged to give us the single GFP fluorescence intensity. This intensity was plugged into a binomial distribution of four fluorescent GFP molecules with a folding efficiency of 74% to get the representative single-channel fluorescence intensity. The GFP intensity of clustered and nonclustered regions of the TIRF footprint were measured and divided by the single-channel fluorescence intensity to obtain the Kv2.1 channel density in these regions. Channel density was multiplied by whole-cell capacitance (C_M), based on voltage-clamp recordings, to extrapolate measurements from the TIRF footprint to the whole cell. The TIRF imaging conditions were carefully optimized to maximize the signal-to-noise of single GFP-Kv2.1 channels while minimizing the total internal reflection (TIR) penetration depth and 488 nm laser intensity to remain within the linear range of the EM-CCD camera (~100–10000). A calculated penetration depth of 144 nm and 10% 488 nm laser intensity satisfied these criteria.

Confocal and TIRF microscopy. HEK cells and neurons expressing fluorescent protein-tagged constructs or immunolabeled with fluorophores were imaged with one of two microscope systems depending on the experiment performed. Standard 3D imaging, 0.3 μm *z*-steps, was performed with an Olympus FV1000 confocal microscope equipped with spectral detectors and the SIM scanner. GFP was excited using the 488 nm line of an argon laser, and emission was collected using the variable bandpass filter set at 500–530 nm. Alexa Fluor 594 fluorophores were detected using a 543 nm HeNe laser with the variable bandpass filter set at 600–700 nm. A 60×, 1.4 NA oil-immersion objective was used for imaging and the pinhole diameter set for the appropriate Airy unit when using one laser. A comprised pinhole diameter was used when two fluorophores were being detected simultaneously. For quantitative imaging, the detector voltage and laser power were kept constant at levels that avoided signal saturation. The second system is a Nikon Eclipse Ti Perfect-Focus equipped TIRF/wide-field fluorescence microscope equipped with AOTF-controlled 405, 488, 561 nm diode lasers, 100 mW each, and an Intensilight wide-field light source. A 100× PlanApo TIRF, 1.49 NA, objective was used for image acquisition. Emission was collected through a Sutter Lambda 10–3 filter wheel containing the appropriate bandpass filters. This microscope is equipped with the Andor iXon EMCCD DU-897 camera, 512×512. For TIRF image acquisition, we used an incident angle of 63.3°, calculated using the following equation: $\mathrm{Sin}\theta = 2 \times R \times M/(200{,}000 \times n_1)$, where R is the distance of the laser illumination position from the center (1360 μm), M is the magnification of the objective (100×), and n_1 is the refractive index of the cover glass (1.522). From the incident angle, the penetration depth was calculated to be 144 nm based on the equation: $d = \lambda/(4\pi \times [n_1{}^2 \times \sin{}^2\theta - n_2{}^2]^{1/2})$, where λ is the laser wavelength (488 nm), θ is the incident light angle to the boundary surface between the cover glass and the culture fluid where $\theta > \theta_c$ (θ_c is the critical angle, $\mathrm{Sin}\theta_c = n_2/n_1$), n_1 is the refractive index of the cover glass, and n_2 is the refractive index of the culture fluid (1.333). At this penetration depth, we rarely observed out-of-focus fluorescence from intracellular sources; however, it is impossible to exclude fluorescence from intracellular organelles near the PM, such as trafficking vesicles and ER. To confirm that our imaging conditions did not typically illuminate intracellular structures, we labeled HEK cells expressing GFP-Kv2.1-HA, containing an engineered extracellular HA epitope in the S1-S2 loop (O'Connell and Tamkun, 2005), with an anti-HA antibody conjugated to Alexa Fluor 594. The ratio of GFP:Alexa Fluor 594 fluorescence was stable at ~5:1 over a range of penetration depths (91–182 nm) but quickly increased to 10:1 when TIR was lost after passing the critical angle (61.1°, data not shown). Furthermore, the relationship between

GFP and Alexa Fluor 594 fluorescence was linear over two orders of magnitude of GFP intensity, within the range of measurements used for quantification of Kv2.1 channel number (see Fig. 5*B*). Previous studies have demonstrated that GFP-Kv2.1 traffics well to the cell surface and does not accumulate in the ER (O'Connell et al., 2006; Tamkun et al., 2007). Although a recycling population of Kv2.1 is present near the PM in endosomal vesicles, these represent <2% of the fluorescence observed under our standard TIRF parameters (Deutsch et al., 2012).

Whole-cell ionic current measurements. HEK cells transfected with fluorescent Kv constructs were trypsinized 24 h after electroporation and replated on 35 mm glass-bottom dishes coated with Matrigel. After 2 h, cells were washed extensively with whole-cell external recording solution, containing (in mM) 140 NaCl, 5 KCl, 10 $CaCl_2$, 2 $MgCl_2$, 10 glucose, and 10 HEPES, pH 7.4. When 20 mM tetraethylammonium chloride (TEA-Cl) was added to the external solution to reduce Kv2.1 currents by ~80%, NaCl was reduced to maintain isotonic conditions. Pipettes were pulled from thin-walled borosilicate glass and had a resistance of 1.4–2.2 MΩ when filled with intracellular solution (150 KCl, 1 $MgCl_2$, 4 NaCl, 0.5 EGTA, and 10 HEPES, pH 7.4). For Kv1.4 current measurements, whole-cell external solution was modified to have 150 mM KCl instead of NaCl, and the intracellular solution was modified to have 100 mM KCl and 50 mM NMDG to reduce the current magnitude.

For measurements in cultured hippocampal neurons, tetrodotoxin (100 nM) was included in the neuronal recording solution (126 NaCl, 2.5 KCl, 1.2 $MgCl_2$, 2.5 $CaCl_2$, 1.2 NaH_2PO_4, 10 HEPES, and 11.1 glucose, pH 7.4) to block voltage-dependent sodium currents. Neuronal intracellular recording solution contained 115 KCl, 20 NaCl, 1.5 $MgCl_2$, 5 HEPES, 0.5 EGTA, and 1.6 K_2ATP, pH 7.4. To determine the contribution of Kv2.1 to the Ik_{DR} in our preparation, we applied the Kv2 family-specific stromatoxin (ScTx) (Alomone Labs), a gating modifier that shifts the activation midpoint of Kv2.1 by +60 mV in HEK cells. At +40 mV, 600 nM ScTx, a concentration reported to block ~75–80% of endogenous Kv2 in neurons (Guan et al., 2007; Guan et al., 2011), blocked Ik_{DR} 125 ms after depolarization by ~47% at 14–15 DIV and by ~46% at 20–21 DIV, indicating that at least half of Ik_{DR} is mediated by Kv2 subunits at both maturity points. Because the dosage of ScTx used here does not fully block Kv2 channels, we increased the contribution of Kv2 to Ik_{DR} to 60% for both time points (47% + (47% × 0.25) = 58.75%). Because Kv2.2 is not significantly expressed in hippocampal neurons, we can exclude the contribution of this channel (Kihira et al., 2010). ScTx also blocks Kv4.3 with a similar affinity as Kv2 subunits; however, this channel is rapidly inactivating and should be largely excluded from Ik_{DR}.

Whole-cell K^+ currents were recorded at room temperature using an Axopatch 200B amplifier (Molecular Devices). Ionic currents were capacitance and series resistance compensated by 80–90%, sampled at 10 kHz (Digidata 1440; Molecular Devices), and filtered at 2 kHz. Leak subtraction was performed online using the P/4 method in pClamp10, but nonsubtracted records were used to assess data quality. Cells were held at −80 mV and depolarized to potentials between −60 and +60 mV in 10 mV steps for 250 ms with an interpulse interval of 10 s. Peak ionic currents were converted to conductance using the equation $G = I/(V - E_K)$. E_K was calculated to be −85 mV. Voltage-activation curves were obtained by plotting peak tail currents obtained at −40 mV against the previous command potential. A standard Boltzmann fit was used to determine the voltage for half-maximal activation ($y = A2 + (A1 - A2)/(1+e^{(x - x0)/dx})$). C_M was automatically calculated from a 10 mV test pulse in pClamp10 and was measured 5 min after break-in to allow cell parameters to stabilize. Current density was calculated by dividing peak current by C_M. When needed, C_M was converted to membrane surface area with the specific capacitance for HEK cells (1.11 $\mu F/cm^2$) and cultured hippocampal neurons (0.92 $\mu F/cm^2$) (Gentet et al., 2000).

One of the inherent drawbacks of measuring large (>10 nA) currents typical of Kv2.1 and Kv1.4 is the potential for voltage error. There is an intrinsic error in the ability of the amplifier to maintain a set voltage where $V_{error} = R_{series} \times I_{clamp}$. Thus, a 1 nA current measured in a cell with 5 MΩ series resistance will produce a voltage error of 5 mV. While all our recordings were performed with series resistance <5 MΩ and series resistance compensation of at least 80%, in a worst-case scenario, a 10 nA current still produces up to 10 mV of voltage error. We minimized voltage error in two additional ways: First, the majority of recordings of Kv2.1 or Kv2.1ΔC current were done in the presence of 20 mM external TEA, which blocks ~80% of the current through Kv2.1 (Immke et al., 1999). Second, we calculated the number of conducting channels from the peak tail currents at −40 mV where the last several tail current tracings had saturated because of complete activation in the previous depolarizing voltage steps to +40 to +60 mV. Relying on tail currents under conditions of maximal activation avoided the need to depend on a determined voltage-activation midpoint, which could be susceptible to voltage error. Together, these approaches allowed us to avoid currents >3.4 nA while measuring conducting channel numbers >78,000. It should be noted that, despite the potential for voltage error, we have no evidence for serious error in the cells used for our analysis. For example, activation midpoints determined by plotting peak tail currents against the previous step depolarization were +3.4 ± 1.4 mV ($n = 21$), whereas the midpoint calculated from traditional G/G_{max} plots was +13.5 ± 1.4 mV ($n = 21$). Both values are in close agreement with previously published values (Shi et al., 1994).

Calculation of endogenous Kv2.1 channel density in cultured hippocampal neurons. We began by calculating Kv2.1 channel density in nonclustered regions of GFP-Kv2.1-transfected HEK cells. Both the transfected HEK cells and cultured hippocampal neurons 14 or 20 DIV were fixed and immunolabeled simultaneously using the same C-terminal monoclonal antibody (NeuroMabs). HEK cells for which channel densities had been calculated from the GFP fluorescence were reimaged on a confocal microscope by capturing a single confocal section through the basal membrane. An ROI was drawn in precisely the same region as had been used to calculate channel density, and the average intensity per micrometer squared was divided by the channel density to obtain the single-channel immunofluorescence in arbitrary fluorescent units (A.U.). Immunolabeled neurons were imaged in the same manner, using the same parameters as with the transfected HEK cells. Neurons cultured for 14 and 20 DIV were handled separately and on different days, so that each group was paired with a different set of HEK cells. Confocal sections through the basal membrane of each neuron were used to measure the immunofluorescence intensity of clusters and noncluster regions. Clusters are defined as local accumulations of fluorescence at least threefold greater than the surrounding fluorescence (cluster fluorescence ranges from 3-fold to tenfold brighter than nonclustered fluorescence, on a cell-to-cell basis). Automated object finding software (Volocity Version 6.0) was used to select and measure clusters. Five ROIs were drawn away from the clusters and averaged to measure nonclustered intensity, and a single ROI drawn around the perimeter of the basal membrane was used to measure total intensity. Cells immunolabeled without the primary antibody were used to subtract nonspecific fluorescence from labeled cells. Each of these measurements was divided first by the area each occupied in micrometers squared and then by the single-channel immunofluorescence to obtain endogenous Kv2.1 density (channels/μm^2). C_M was used to define the plasma membrane surface area such that our comparison of current density and total channel number relies on the assumption that the measured C_M is an accurate measurement of membrane surface area. The mean C_M for DIV 14 neurons was 56.5 ± 2.6 pF, which is in agreement with other C_M measurement for pyramidal hippocampal neurons in culture (Yang et al., 1993). However, a rat postnatal day 14 (P14) freshly dissociated neuron cell body has a C_M of 14.3 ± 3.8 pF (Guan et al., 2011), suggesting that much of the C_M can be attributed to the neurites, and it is unclear how much electrical access exists into these compartments. Our assumption is that we can measure currents over the same membrane surface from which the C_M measurement is derived.

Our findings also rely on the assumption that immunolabeling performed at the same time with the same solutions will generate the same efficiency of antibody binding to Kv2.1 channels whether they are expressed in an HEK cell or a neuron. Although we cannot be positive that the antibody binding efficiency is identical in HEK cells and neurons, we can make other assumptions about the labeling efficiency. HEK cells have a simple geometry lacking extensive compartmentalization and are plated at low density, providing space between each cell. Neurons instead have an extremely complex morphology and typically grow in dense networks of neuropil, which could obstruct antibody access or lower the relative concentration of antibody. Thus, if a difference in antibody labeling

efficiency exists, it is most likely to be in favor of labeling in HEK cells. This sort of a discrepancy would underestimate the number of Kv2.1 channels expressed endogenously in cultured hippocampal neurons and would only further support our conclusion that a significant nonconducting Kv2.1 population exists in neurons.

Image presentation and data analysis. Images were imported into Volocity Version 6.0 software for contrast enhancement, 3D reconstruction, object detection, and quantitative analysis. Numerical data were exported into Origin Pro 8.5 for further analysis, curve fitting, and figure preparation. Compilation of images was performed using Adobe Illustrator, and contrast and brightness adjustments were made. Both compressed (maximum projection) and single Z-section images are displayed as indicated.

Statistics. Data are presented as mean ± SEM. Statistical analysis was performed using an unpaired or paired *t* test, with $p < 0.05$ considered statistically significant, as indicated in the figure legends.

Results

Kv2.1 partitions equally between clustered and nonclustered cell-surface domains in HEK cells

Using a combination of TIRF microscopy and laser scanning confocal microscopy, we first determined the whole-cell distribution of GFP-Kv2.1 in transfected HEK cells. Figure 1*A* shows a maximum projection confocal *z*-stack of an HEK cell transfected with an N-terminal GFP fusion of Kv2.1. These clusters are indistinguishable from endogenous Kv2.1 clusters in neurons (O'Connell et al., 2006). The mean intensity from the basal membrane of a randomly selected population of immunolabeled HEK cells transfected with Kv2.1 (497 ± 26.4 A.U./pixel, $n = 15$, data not shown) was only approximately twofold greater than that of endogenous Kv2.1 (255.4 ± 36.3 A.U./pixel, $n = 11$, data not shown) in DIV 20–22 neurons. Thus, Kv2.1 localization in HEK cells does not represent an overexpression artifact. Figure 1*B* shows a TIRF image of the basal surface of a GFP-Kv2.1 expressing HEK cell where both clustered and nonclustered Kv2.1 expression is observed. We define clusters as having at least >3-fold fluorescence than the surrounding area, although this ranges from threefold to tenfold from cell to cell. In this particular cell, the Kv2.1 clusters occupied 15% of the total footprint surface area and contained 5.4-fold greater fluorescence intensity than nonclustered membrane with 48% of the total fluorescence restricted to clusters. The average cluster intensity in this cell was 4938 ± 123 A.U./pixel. The small SE indicates that the density of channels within clusters is very consistent. Overall, the GFP-Kv2.1 clusters accounted for 20% of the basal surface area and 52 ± 3.8% of the total fluorescence, whereas nonclustered GFP-Kv2.1 accounted for 45.6 ± 3.3% of the total fluorescence ($n = 21$). Thus, the Kv2.1 clusters on the basal surface contain approximately an equal number of channels compared with the nonclustered membrane.

The quantitation thus far considers only the basal surface of the cell directly in contact with the coverslip. Whether the clusters have a preference for the top or the bottom of the HEK cell was not known. To address this question, HEK cells expressing GFP-Kv2.1 were labeled with DiI to provide an unbiased measure of total membrane surface area after confocal imaging and 3D reconstruction. A representative 3D reconstruction from confocal *z*-sections illustrating the top and bottom of the same cell is shown in Figure 1*C* and Figure 1*D*, respectively. Here the GFP-Kv2.1 clusters (green) are shown against total membrane labeled with DiI (red). Automated object finding (Volocity Version 6.0) was used to measure the volume of either the total membrane (DiI) or just the Kv2.1 clusters (GFP). The percentage of membrane volume occupied by clusters in this cell was 14%. Overall, 19 ± 1.7% ($n = 5$) of the cell surface was cluster-occupied,

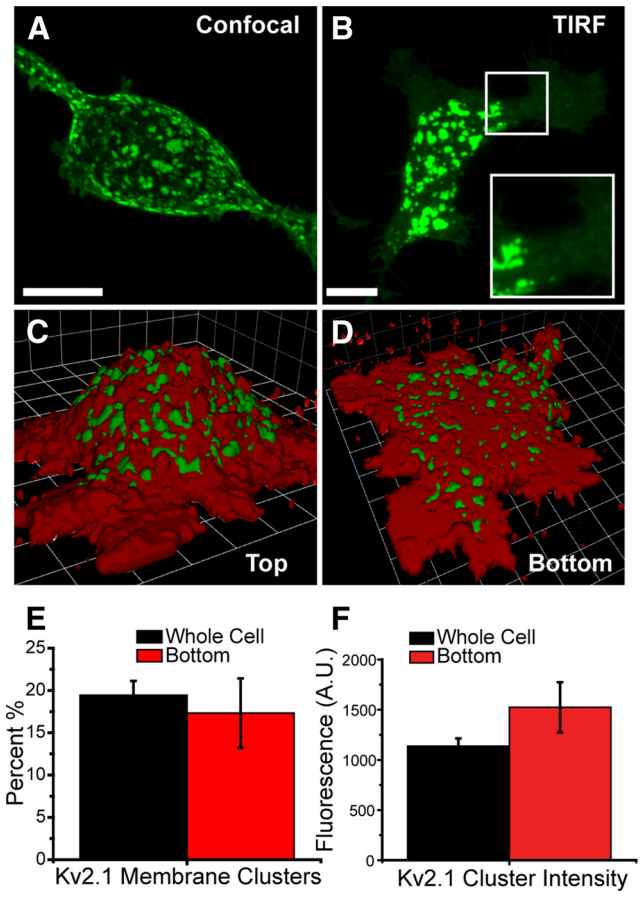

Figure 1. GFP-Kv2.1 localizes to dense cell-surface clusters in transfected HEK cells. ***A***, Compressed (maximum projection) confocal *z*-stack of an HEK cell transfected with an N-terminal GFP fusion of Kv2.1. These clusters are indistinguishable from endogenous Kv2.1 clusters in neurons. ***B***, HEK cell transfected with GFP-Kv2.1 and imaged using TIRF microscopy. The nonclustered population of Kv2.1, which is evenly distributed on the membrane, is more readily visible in TIRF. Inset, Magnified and enhanced contrast of the white boxed ROI. Scale bar, 10 μm. ***C***, ***D***, Three-dimensional reconstruction of an HEK cell transfected with GFP-Kv2.1 and the plasma membrane stained with DiI as seen from the top (***C***) and bottom (***D***). Confocal *z*-stacks were reconstructed using Volocity Version 6 software. Each grid = 5.29 μm. ***E***, Graph comparing the percentage of basal membrane occupied by Kv2.1 clusters (19 ± 2%, red) with the percentage of membrane cluster occupied at the whole-cell level (17 ± 3%, $n = 5$, black). Percentage of membrane occupied by Kv2.1 clusters was determined using an automated analysis in Volocity Version 6 where total membrane volume was obtained from DiI labeling and Kv2.1 clusters were detected based on GFP fluorescence. ***F***, Graph comparing the intensity of Kv2.1 clusters on the bottom of the cell (1520 ± 250, red) with those present over the cell as a whole (1140 ± 80, black) (paired *t* test, $p = 0.14$).

and there was no difference between the bottom of the cell and the whole cell (Fig. 1*E*). Furthermore, the density of cluster GFP in Figure 1*C*, *D* was similar between clusters within the same cell and averaged 6.2 ± 0.7-fold ($n = 5$) greater than the density in the surrounding cluster-free membrane. The cluster intensity on the bottom of the cell (1524 ± 250 A.U./pixel) tended to be greater than the whole cell (1136 ± 78 A.U./pixel), but this difference was not significant (paired *t* test, $p = 0.14$, $n = 5$; Fig. 1*F*). Thus, the TIRF image of the basal membrane shown in Figure 1*B* is representative of the entire cell surface.

Detection of individual GFP-tagged Kv2.1 channels in HEK cells

Our previous findings with on-cluster cell-attached patch-clamp experiments indicate that Kv2.1 channels retained within clusters

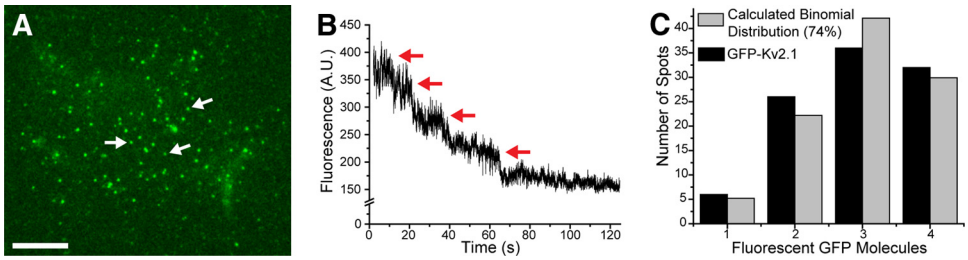

Figure 2. Stepwise bleach of individual GFP-Kv2.1 channels. HEK cells transfected with GFP-Kv2.1 were imaged using TIRF microscopy and an EM-CCD camera. ***A***, HEK cell expressing low numbers of GFP-Kv2.1 channels. White arrows point to discrete GFP puncta associated with a single Kv2.1 channel. ***B***, Graph of the fluorescence of a single GFP-Kv2.1 puncta over time. Photo-bleaching occurs in four discrete steps as indicated by the red arrows. ***C***, Graph of the distribution of fluorescent GFP molecules per discrete fluorescent puncta ($n = 100$) (black bars). The distribution of a binomial distribution (gray bars) assuming a GFP folding efficiency of 74% is presented for comparison. Scale bar, 10 μm.

do not open in response to positive voltage steps in contrast to the nonclustered channels that behave like the archetypal Kv2.1 delayed rectifier (O'Connell et al., 2010). However, there remains the question of whether a subpopulation of nonconducting channels exists outside the Kv2.1 clusters. To address this issue, we determined the number of Kv2.1 molecules within and outside the surface clusters and compared this Kv2.1 channel number with whole-cell current magnitude.

Channel number can be calculated from the TIRF footprint of a GFP-Kv2.1 expressing HEK cell if the intensity of a single tetrameric GFP-Kv2.1 channel is known. TIRF-based photo-bleach was used to monitor the stepwise bleach of discrete fluorescent puncta during continuous illumination in the same manner used to determine subunit stoichiometry (Leake et al., 2006; Ulbrich and Isacoff, 2007). Because the tetrameric Kv2.1 contains up to four functional GFP molecules, the fluorescence should bleach over time in up to four distinct steps if a single-channel molecule is imaged. We reduced the expression level of GFP-Kv2.1 to the point where only a small number of discrete spots were visible in TIRF illumination, as illustrated in Figure 2*A*. The mobility of these puncta matched the single Kv2.1 channel diffusion characteristics previously reported (Tamkun et al., 2007; Weigel et al., 2011). To confirm that these spots represent single Kv2.1 channels, we plotted the fluorescence intensity of a single spot during constant high-power illumination. The data show a clear four step decrease in intensity indicating that four GFP molecules are present in this diffraction limited spot (Fig. 2*B*). Thus, the mean bleach-step magnitude provides an estimate of the single GFP fluorescence under these imaging conditions. Comparison of single GFP fluorescence with the total fluorescence of 100 discrete GFP-Kv2.1 channels provided an estimate of the number of properly folded, and thus fluorescent, GFP molecules per channel. Single GFP-Kv2.1 channels frequently had either four (32%) or three (36%) functional GFP molecules. Less frequently, two (26%) or one (6%) GFP molecules were detected, as summarized in Figure 2*C*. This is consistent with an independent GFP folding efficiency of ~74% and is in agreement with the measured folding efficiency in other fluorescent protein fusions (Sugiyama et al., 2005; Ulbrich and Isacoff, 2007; Plant et al., 2011). Thus, we can readily determine the fluorescence intensity of both single GFP molecules and tetrameric GFP-Kv2.1 channels in addition to the efficiency of GFP folding in the GFP-Kv2.1 fusion.

Measurement of GFP-Kv2.1 channel cell surface density using single-channel fluorescence and TIRF microscopy

The single molecule fluorescence intensity values discussed above were next used to calculate Kv2.1 molecule density from the membrane GFP fluorescence measured during TIRF imaging. However, in HEK cells expressing sufficient Kv2.1 channels to visualize the formation of clusters, it was impossible to identify discrete GFP-Kv2.1 channels, necessitating the measurement of the single channel or single GFP intensity in a different cell. The intensity of the TIRF evanescent wave decays exponentially as the distance from the coverslip increases (i.e., very small deviations in the distance between the cell and the coverslip are magnified into large differences in illumination and subsequent emission intensity) (Mashanov et al., 2003). To control for variations in illumination intensity, we transfected cells with either high (3 μg) or low (0.5 μg) quantities of plasmid DNA and then plated these cells together in the glass bottom culture dishes used for TIRF imaging (Fig. 3*A*). Assuming that adjacent cells have minimal variations in distance from the coverslip, they will receive equivalent illumination. Single-channel fluorescence measurements were made from cells expressing low numbers of GFP-Kv2.1 channels and the single-channel fluorescence (Fig. 3*A*, white arrows) was used to calculate channel density (channels/μm^2) in an adjacent cell expressing a much greater number of channels (Fig. 3*A*, red arrow). In this manner, every Kv2.1 surface density determination had its own internal standard. Cells were selected based on fluorescence intensity to encompass the entire spectrum of expression levels. This quantitation was performed in conjunction with K^+ current density measurements via whole-cell voltage clamp of the same cell being imaged for the fluorescence-based channel density determination.

Estimation of GFP-Kv2.1 conducting channel number using whole-cell K^+ current amplitude

Calculating the absolute number of conducting Kv2.1 channels in transfected HEK cells requires an accurate measurement of the total whole-cell current, the single-channel conductance and the opening probability (P_O) at the membrane potential used. The single-channel conductance of Kv2.1 has been extensively studied (Trapani et al., 2006) and was calculated to be 6.15 pS in 5 mM external K^+, whereas the maximum P_O was 0.7 (Islas and Sigworth, 1999). Whole-cell currents in voltage clamp were measured during 250 ms step depolarizations from a holding potential of −80 mV to +60 mV in 10 mV increments (Fig. 3*D*). Deactivating tail currents were recorded at −40 mV. The level of expression required to visualize cluster formation in HEK cells that mimics that of the endogenous channel in hippocampal neurons results in whole-cell K^+ currents >10 nA in amplitude. Therefore, recording accurate whole-cell currents for Kv2.1 under conditions favoring cluster formation is difficult because of high peak current levels in addition to the series resistance/voltage error concerns. The primary concern is that these current levels can result in a loss of voltage control because the active

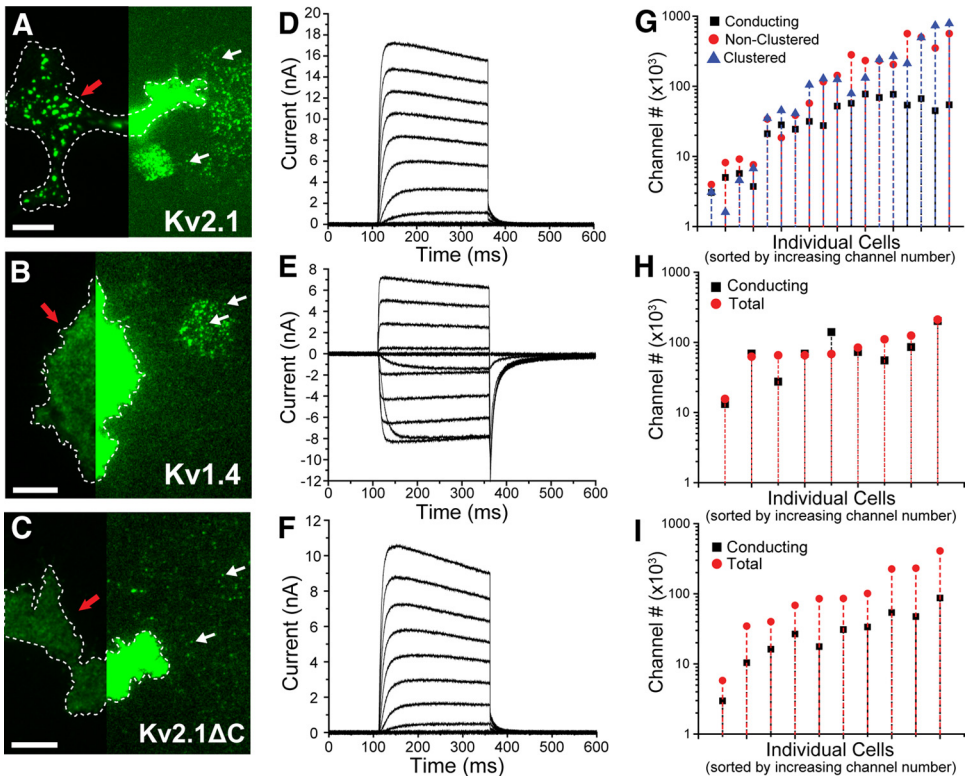

Figure 3. Simultaneous TIRF imaging and whole-cell voltage clamp. ***A–C***, HEK cells were transfected with high and low concentrations of Kv2.1 (***A***), Kv1.4 (***B***), or Kv2.1ΔC (***C***) GFP fusions and plated together to achieve both expression levels in one field of view (each panel has two transfected cells, side by side). Cells used for voltage clamp (red arrows) were too bright to discern single GFP-tagged channels. The contrast in the right half of each image was enhanced, so single GFP-tagged channels (white arrows) from an adjacent cell expressing a low number of channels were visible. ***D–F***, Whole-cell voltage clamp recordings of Kv2.1 (***D***), Kv1.4 (***E***), and Kv2.1ΔC (***F***) in response to 250 ms voltage steps ranging from +60 to −60 mV (+40 to −80 mV for Kv1.4) in 10 mV increments. After each voltage step, tail currents were measured at −40 mV (Kv2.1 and Kv2.1ΔC) and −60 mV (Kv1.4) to assess channel activation. The high external K^+ solution used to record Kv1.4 currents causes the reversal potential to shift to ~+7 mV. ***G***, Quantification of nonclustered (circle), clustered (triangle), and conducting (square) Kv2.1 channel number for individual cells sorted by increasing channel number. Note the log scale for the *y*-axis. ***H***, ***I***, Quantification of total (circle) and conducting (square) channel number for Kv1.4 (***H***) and Kv2.1ΔC (***I***). Individual cells are sorted by increasing channel number. Note that the number of total and conducting channels are consistently similar (1.24 ± 0.16, $n = 9$) for Kv1.4, whereas total channel number is in excess relative to conducting Kv2.1 and Kv2.1 ΔC number. Scale bar, 10 μm.

outward flow of K^+ ions at depolarized potentials tends to hyperpolarize the actual membrane potential relative to the command potential. Collapsing the transmembrane K^+ gradient by elevating extracellular K^+, and thus reducing the driving force and current magnitude, was not a viable option because Kv2.1 single-channel conductance increases with increasing extracellular K^+ (Trapani et al., 2006). Voltage error was minimized by using only cells with a total access resistance < 5 MΩ and by careful use of 80–90% series resistance compensation. We further reduced potential voltage clamp error in two ways. First, the vast majority of recordings were made in the presence of 20 mM TEA to block 78 ± 4% ($n = 4$, data not shown) of the whole-cell current, consistent with previous reports (Immke et al., 1999). Second, in our data analysis to calculate conducting channel number, we used the peak tail current measured at −40 mV, a potential where the K^+ currents are smaller because of reduced driving force, and variations in activation midpoint are not significant as maximal activation has been achieved. Using these approaches allowed us to detect up to 78,000 conducting channels per cell without relying on whole-cell K^+ current amplitudes >3.4 nA. Thus, for a given cell, we were able to measure the Kv2.1 channel density within clusters and outside clusters based on GFP fluorescence while in the same cell simultaneously calculating total conducting channel number based on current measurements under whole-cell voltage clamp. For each cell, channel densities obtained from the TIRF-derived basal membrane GFP fluorescence were extrapolated to account for the entire cell membrane using the membrane C_M obtained during voltage clamp in conjunction with the measurements of the Kv2.1 cluster distribution obtained in Figure 1.

The percentage of nonconducting Kv2.1 channels is highly variable

Figure 3*G* compares the number of Kv2.1 channels on individual HEK cell surfaces in either clusters (triangle) or noncluster membrane (circle) (as obtained from the GFP fluorescence illustrated in Fig. 3*A*) to the whole-cell currents (square) (shown in Fig. 3*D*). Individual cells ($n = 21$) are sorted by increasing total channel number and symbols along each vertical line represent measurements from the same cell. Overall, the average number of conducting channels was 39,000 ± 6000, and there were 187,000 ± 46,000 nonclustered and 191,500 ± 57,000 clustered Kv2.1 surface molecules ($n = 21$). These data indicate that the majority of Kv2.1 channels are held in a nonconducting state. As illustrated in Figure 3*G*, this trend does not hold for every cell because at the lower expression levels there is closer agreement between the number of nonclustered channels and the K^+ current. However, as the expression level increases, only a fraction of the nonclustered channels can be conducting. At the highest expression levels, the number of conducting channels appears to saturate, perhaps indicating an absolute limit of channel conductance (Fig. 3*G*). There was no relationship between the levels of

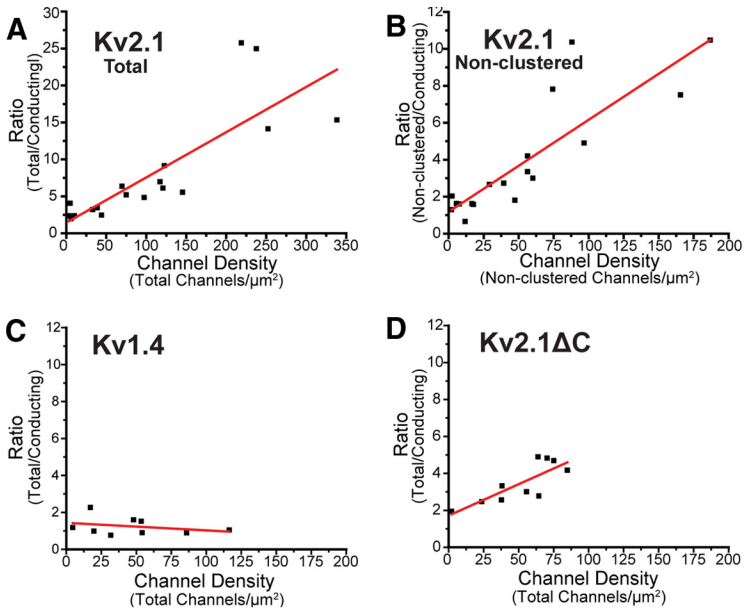

Figure 4. The fraction of Kv2.1 nonconducting channels increases as channel density increases. ***A***, Ratio of total Kv2.1 channel molecules (calculated from single-channel fluorescence) to conducting channels (calculated from whole-cell currents) plotted as a function of total channel density (intercept = 1.44, $R^2 = 0.65$). ***B***, Ratio of nonclustered channel number to conducting channels plotted as a function of nonclustered channel density (intercept = 1.18, $R^2 = 0.72$). ***C***, ***D***, Ratio of total Kv1.4 (***C***; intercept = 1.72, $R^2 = 0.6$) and Kv2.1ΔC (***D***; intercept = 1.43, $R^2 = -0.04$) channel number to conducting channels plotted as a function of total channel density. For Kv2.1 (***A***, ***B***) and Kv2.1ΔC (***D***), the ratio increases as density increases, whereas for Kv1.4 (***B***) the ratio remains ~1:1 at all densities measured. Red lines indicate linear fits using the equation $y = a + b \times x$.

GFP-Kv2.1 expression and the activation midpoint measured from tail currents (mean = +3.4 ± 1.4 mV, $n = 21$, data not shown). Our original hypothesis predicted a good agreement between nonclustered and conducting channel values, whereas clustered channel numbers were expected to have no relationship to either. Instead, we found that high expression levels decreased the percentage of nonclustered channels conducting K^+.

Nonconducting state of GFP-Kv2.1 is density dependent

Figure 4*A* summarizes the relationship between expression density and channel conductance for the wild-type Kv2.1. Here, the conducting ratio, obtained by dividing the number of total Kv2.1 channels by the number of conducting channels, is plotted against Kv2.1 plasma membrane expression density in the same cell. A ratio of 1 indicates that all expressed channels are functional, whereas a ratio of 2 indicates that half of the expressed channels are nonconducting. Figure 4*A* illustrates that as the total density of channels increases there is a clear trend toward greater ratios, indicating that there is indeed an effect of expression level on the nonconducting state. Figure 4*B* plots the conducting ratio for only nonclustered channels against the expression density of those channels. The trend here again indicates that the density of nonclustered channels determines what fraction of these channels is nonconducting. Because the conducting ratio approaches 1 at the lower expression levels, most of the nonclustered channels are conducting. In summary, the nonconducting state of Kv2.1 is dependent on the density of channel expression regardless of whether or not the channels are located within a cluster microdomain.

Kv1.4 conductance is not affected by channel density

To assure that the density-dependent nonconducting state observed for GFP-Kv2.1 was not related to unknown error in our channel counting technique, we performed the same analysis on HEK cells transfected with GFP-Kv1.4. Unlike Kv2.1, GFP-Kv1.4 has unrestricted mobility on the cell surface and a homogeneous surface localization (Tamkun et al., 2007). Therefore, we measured the GFP density from an ROI encompassing the entire TIRF footprint (Fig. 3*B*). Because Kv1.4 is insensitive to TEA ($IC_{50} >$ 100 mM), we altered the potassium gradient (150 mM K^+ outside/100 mM K^+ inside) to minimize whole-cell current amplitude (Fig. 3*E*) and ensure proper voltage control (Stuhmer et al., 1989). Much like Kv2.1, Kv1.4 is modulated by external potassium. However, unlike Kv2.1, increasing external potassium increases the P_O of the Kv1.4 channel and not the single-channel conductance with P_O reaching a maximum of 0.8 in the presence of 100 mM external K^+ (Pardo et al., 1992). The voltage-step protocol to generate currents was similar to that used for Kv2.1, and the peak tail current amplitude measured at −60 mV was used to calculate conducting channel number. Nearly identical conducting channel numbers were also calculated when using the slightly smaller outward currents generated at either +30 or +40 mV, potentials where channel activation is maximal. The relationship between Kv1.4 channel number and conductance is summarized in Figure 3*H*, which shows consistent agreement between channel number based on GFP fluorescence and channel number based on current. The mean conducting ratio for Kv1.4 was 1.24 ± 0.16 ($n = 9$), indicating that there is no significant nonconducting population of Kv1.4 channels. The plot of conducting ratio against channel density shown in Figure 4*C* demonstrates that, for all individual cells, the conducting ratio is ~1, regardless of the expression level. In summary, when we apply the channel counting technique to a Kv subunit for which there is no previous evidence of a large nonconducting population, we obtain nearly perfect agreement between conducting channel number and expressed channel number.

Kv2.1 nonconducting state is independent of both clustered localization and the channel C terminus

Although the Kv2.1 nonconducting state originally appeared related to cluster localization (O'Connell et al., 2010), the summary shown in Figure 4*B* suggests that this localization per se is not responsible for the lack of channel activity. Domains in both the amino and C termini of Kv2.1 are necessary for its localization to clusters (Lim et al., 2000; Mohapatra et al., 2008). Although the most critical residues have been mapped to the proximal regulation of clustering domain on the C terminus, removal of the entire C terminus is a simple way to eliminate cluster localization (Lim et al., 2000). As illustrated in Figure 3*C*, a mutant Kv2.1 in which the last 318 amino acids were deleted (GFP-Kv2.1ΔC) fails to form the classic Kv2.1 clusters. Because GFP-Kv2.1ΔC is localized diffusely over the membrane surface, we measured channel density from a single ROI encompassing the entire TIRF footprint, as was done for GFP-Kv1.4. Figures 3*I* and 4*D* summarize the relationship between channel number and current. Even at the lowest expression level, only half of the GFP-Kv2.1ΔC chan-

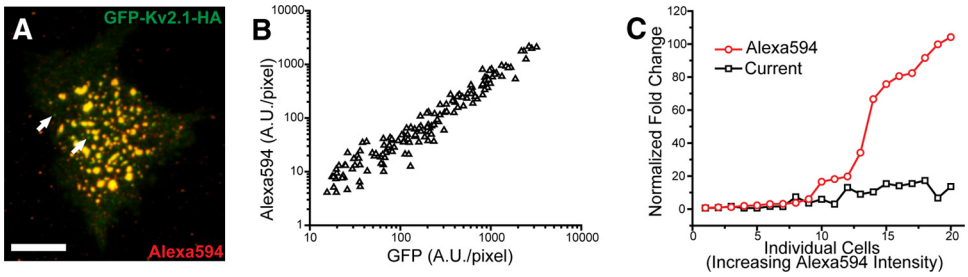

Figure 5. Nonconducting Kv2.1 channels reside on the cell surface. ***A***, HEK cell expressing GFP-Kv2.1-HA and labeled with an anti-HA antibody conjugated to Alexa Fluor 594 (1:1000). White arrows point to unlabeled GFP spots, which are likely intracellular vesicles and account for ~0.4% of the total GFP fluorescence from the TIRF footprint. Scale bar, 10 μm. ***B***, The GFP and Alexa Fluor 594 intensity from 147 cells is plotted. The relationship is linear over the range of GFP intensities used in this study. ***C***, Whole-cell current and Alexa Fluor 594 intensity were measured for 20 cells spanning a large range of expression levels and normalized to the average of the three lowest expressing cells. At higher expression levels, there is a much greater fold increase in Alexa Fluor 594 than whole-cell current.

nels are conducting, much like the total population of wild-type GFP-Kv2.1. As the expression of GFP-Kv2.1ΔC increases, there is a concomitant increase in the percentage of nonconducting channels; however, the slope of this relationship (0.034 ± 0.01, $n = 9$) is approximately half that of wild-type GFP-Kv2.1 (0.061 ± 0.01, $n = 21$). Aside from the absence of clusters with the GFP-Kv2.1ΔC channel, the most notable difference from the wild-type channel is the maximum channel density. The highest channel density measured for the GFP-Kv2.1ΔC channel was 85 channels/μm^2, less than half the highest density of nonclustered GFP-Kv2.1 (187 channels/μm^2). It is not surprising that GFP-Kv2.1ΔC was unable to achieve surface expression levels equal to GFP-Kv2.1 given the role of the C terminus in efficient trafficking (Mohapatra et al., 2008). The lower cell-surface expression of GFP-Kv2.1ΔC may explain why the percentage of nonconducting channels is less than in cells expressing the wild-type GFP-Kv2.1. Furthermore, this is consistent with a density-dependent mechanism underlying generation of the nonconducting state. These data obtained with the GFP-Kv2.1ΔC channel suggest that neither retention within a cluster nor the C-terminal tail of Kv2.1 is required for the nonconducting state. This is consistent with a recent report demonstrating that, although the C-terminus of Kv2.1 is necessary for clustered localization, it is dispensable with respect to modulation of channel function (Baver and O'Connell, 2012). Together, the data summarized in Figures 3 and 4, argue that (1) the functional state of Kv2.1 is related to the membrane density, (2) the nonconducting state of Kv2.1 is not a direct consequence of cluster residence, and (3) density-dependent regulation of Kv2.1 does not involve the C-terminal 318 amino acids.

Nonconducting Kv2.1 channels reside on the cell surface

Although TIRF microscopy is an excellent method for observing fluorescence at or near the PM, it does not exclude intracellular sources of fluorescence from near-membrane organelles, such as docked trafficking vesicles and cortical endoplasmic reticulum. Although TIRF measurements of GFP-Kv2.1 channel density were carefully made to avoid intracellular fluorescence as discussed in Materials and Methods, we sought to confirm our previous results using a true cell-surface fluorophore. We expressed GFP-Kv2.1-HA, which contains a HA epitope engineered into the S1-S2 extracellular loop (O'Connell and Tamkun, 2005), in HEK cells and labeled with an anti-HA antibody conjugated to Alexa Fluor 594. In Figure 5*A*, there is excellent overlap between GFP and Alexa Fluor 594, and this is especially noticeable in the clusters. Upon closer examination, there are a few GFP spots that do not label with Alexa Fluor 594 (Fig. 5*A*, white arrows). These spots are very likely mobile trafficking vesicles that we have observed previously (Deutsch et al., 2012) and importantly only account for ~0.4% of the total GFP fluorescence of the TIRF footprint in this cell (data not shown). In Figure 5*B*, the fluorescence intensity of GFP and Alexa Fluor 594 from the TIRF footprint of 147 HEK cells transfected with GFP-Kv2.1-HA is shown. Although there is significant spread of the intensities, indicating variability in the labeling efficiency from cell to cell, there is a consistent linear trend over the entire range of GFP intensities used in the previous experiments. This rules out the possibility of an intracellular buildup of GFP-Kv2.1-HA at higher expression levels because this would cause an increase in GFP intensity without a concomitant increase in Alexa Fluor 594 intensity, causing the scatter plot to plateau. Because there is a linear relationship between GFP-Kv2.1-HA expression and Alexa Fluor 594 labeling, we used the Alexa Fluor 594 intensity alone to corroborate our previous results. It is unlikely that Alexa Fluor 594 labels GFP-Kv2.1-HA channels with 100% efficiency, so we cannot use this fluorophore to directly calculate channel density. Instead, we performed paired TIRF imaging and voltage clamp of individual cells spanning a large range of expression levels and then normalized each cell to the average of the three cells with the lowest expression levels. In Figure 5*C*, normalized whole-cell current and normalized Alexa Fluor 594 increase concomitantly at the lower expression levels (cells sorted left to right based on increasing Alexa Fluor 594 intensity). At higher expression levels, very large Alexa Fluor 594 fold intensity increases are contrasted by very small fold increases in whole-cell current. These data agree with the trend shown in Figures 3 and 4: at high expression levels, an increasing proportion of Kv2.1 channel are nonconducting.

Calculation of endogenous Kv2.1 channel density in cultured hippocampal neurons

HEK cells provide an ideal expression system in which to study Kv2.1 due to the neuron-like cell-surface expression pattern after Kv2.1 transfection and the lack of endogenous Kv2.1. However, a HEK cell cannot replicate the entire milieu of neuronal proteins or the complex regulation a neuron exerts over those proteins. Therefore, it was important to determine whether the endogenous neuronal Kv2.1 channels also possess the nonconducting state. To characterize the cell surface distribution of the endogenous Kv2.1 channel in cultured hippocampal neurons, the plasma membrane was first labeled with FITC-conjugated wheat germ agglutinin to provide an unbiased measure of the soma and proximal dendrites over which Kv2.1 clusters were detected. After fixation and detergent permeabilization, Kv2.1 was detected using a monoclonal antibody directed against an epitope within the C terminus and an Alexa Fluor 594-

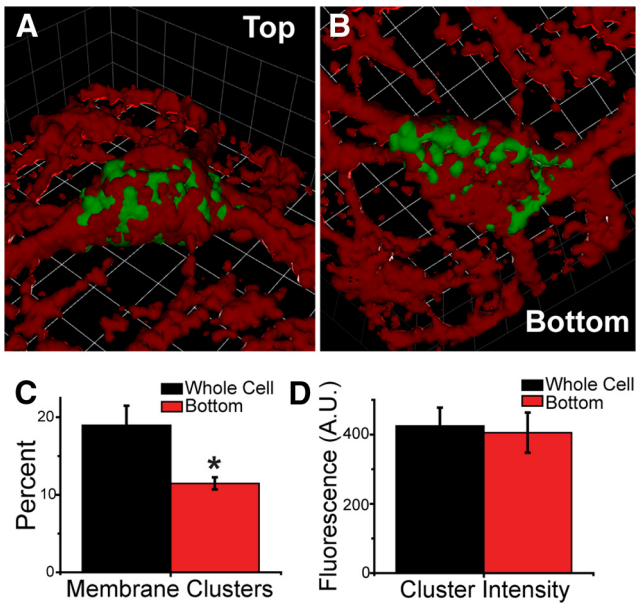

Figure 6. Three-dimensional reconstruction of Kv2.1 plasma membrane distribution in cultured hippocampal neurons. ***A***, ***B***, Fourteen DIV E18 rat hippocampal neurons stained with WGA (red), fixed and immunostained for Kv2.1 (green). Confocal *z*-sections were reconstructed in three dimensions using Volocity Version 6 software. Each grid = 4.21 μm. ***C***, Comparison of the percentage of membrane occupied by Kv2.1 clusters from the bottom of the cell (12 ± 1%, n = 5, red) to the whole cell (19 ± 3%, black). *$p < 0.05$. Percentage of membrane occupied by Kv2.1 clusters was determined using an automated analysis in Volocity Version 6 where total membrane volume was obtained from WGA labeling and Kv2.1 clusters were detected based on antibody fluorescence. Intracellular fluorescence was removed to within 1 μm of the membrane for both labels before automated analysis. ***D***, Comparison of the intensity of Kv2.1 clusters on the bottom of the cell (410 ± 60, red) to the whole cell (420 ± 50, black).

conjugated secondary antibody. 3D reconstructions from confocal *z*-sections are shown in Figure 6*A*, *B*. The endogenous Kv2.1 clusters occupied 19.5% of the soma membrane in this particular neuron, and the immunolabeling within the clusters was 3.95-fold greater than the surrounding membrane. Overall, in the five cells examined, 19.0 ± 2.5% of the soma was cluster occupied with an average density 3.7 ± 0.5-fold greater than the adjacent membrane (n = 5). Although the clusters did occupy a significantly smaller percentage of the basal cell membrane compared with the rest of the soma (Fig. 6*C*), the intensity of the clusters was the same over the entire cell surface (Fig. 6*D*). These data clearly demonstrate that HEK cells faithfully reproduce the localization of endogenous Kv2.1 in cultured neurons.

Next, we developed a method to quantify the endogenous expression of Kv2.1 in cultured hippocampal neurons (Fig. 7*A*). We began by using TIRF microscopy to measure the single-channel fluorescence intensity of GFP-Kv2.1 in HEK cells and used this to calculate channel density (channels/μm^2) essentially as described in previous sections (Fig. 7*B*). These HEK cells were fixed and immunolabeled for Kv2.1 alongside cultured hippocampal neurons either 14 or 20 DIV. A confocal microscope was used to image anti-Kv2.1 immunolabeling of HEK cells, which had previously been imaged using TIRF microscopy (Fig. 7*C*). The immunofluorescence density (A.U./μm^2) of a nonclustered region was divided by the Kv2.1 channel density (channels/μm^2) from the same region to calculate the equivalent of single-channel immunofluorescence (A.U./channel). Transfected HEK cells handled in this way were processed and imaged alongside groups of neurons, either 14 or 20 DIV, so that each neuron group had an internal HEK-based control for Kv2.1 immunofluorescence. In cultured hippocampal neurons, a single *z*-section through the bottom of the cell was used to measure Kv2.1 immunofluorescence from both clustered and nonclustered regions, as well as a single ROI encompassing the entire footprint of the cell to measure total immunofluorescence (Fig. 7*D*). Each measurement was divided by the equivalent of single-channel immunofluorescence to calculate the density of endogenous Kv2.1. The values for the endogenous Kv2.1 density obtained in the manner described above are summarized in Table 1. Thus, by comparing relative Kv2.1 immunofluorescence intensity between transfected HEK cells and cultured hippocampal neurons, we obtain a reasonable estimate of the endogenous Kv2.1 membrane density inside and outside the cluster perimeter.

Endogenous Kv2.1 in hippocampal neurons demonstrates the nonconducting state

Whole-cell electrophysiology was used to measure endogenous K^+ currents from neurons in culture for 14 and 20 d before the immunolabeling described above. Kv2.1 is reported to mediate between 50 and 80% of the delayed rectifier current in principal neurons of the hippocampus and cortex (Murakoshi and Trimmer, 1999; Malin and Nerbonne, 2002; Guan et al., 2007). Both cell ages showed inactivating A-type current superimposed on the delayed rectifier as illustrated in Figure 7*E*. ScTx, a gating modifier that shifts the activation midpoint of Kv2.1 by +60 mV (Guan et al., 2011), blocked the Ik_{DR} at +40 mV by ~47% at 14–15 DIV and by ~46% at 20–21 DIV, indicating at least half of Ik_{DR} was mediated by Kv2 subunits under our culture conditions. Because the dose of ScTx used here only blocks 75–80% of Kv2 channel at +40 mV (Guan et al., 2007), for our calculations we conservatively increased of the contribution of Kv2 to Ik_{DR} to 60% for both time points. Peak Ik_{DR} was measured 125 ms after the beginning of a +40 mV step depolarization to eliminate rapidly inactivating K^+ currents, and tail currents were monitored to ensure that the delayed rectifier Kv currents had attained maximum activation. We then estimated the number of conducting Kv2.1 channels by dividing 60% of the Ik_{DR} by the single-channel current. Finally, we divided the number of conducting channels by the measured whole-cell capacitance (C_M) to estimate conducting channel surface density.

As summarized in Figure 7*F*, the density of conducting Kv2.1 channels was 228 ± 27 channels/pF at 14 DIV and 361 ± 67 channels/pF at 20 DIV. The apparent increase in conducting channel density between DIV 14 and DIV 20 was not significant (p = 0.09). In contrast, there were 1708 ± 200 and 1360 ± 120 total Kv2.1 channels/pF based on the standardized immunolabeling at 14 and 20 DIV, respectively. Thus, the data suggest that, at both maturity levels, there was a large population of expressed channels that were not conducting K^+. If we assume all clustered channels to be nonconducting, on 14 DIV only one in three nonclustered channels would need to be conducting to generate the observed currents. On 20 DIV, approximately two-thirds of the nonclustered channels would need to be conducting because at this age a greater percentage of the Kv2.1 resides within the cluster microdomains. Regardless, there is a clear overabundance of total Kv2.1 surface channel in relation to current at both neuronal ages. These data also suggest that in neurons a portion of nonclustered channels are held in a nonconducting state, which is consistent with our findings in transfected HEK cells at the higher expression levels.

Discussion

This study further examines the relationship between cluster localization and channel function, specifically asking whether nonconducting channels also exist outside the cluster microdomains. Previous work showed that the Kv2.1 channels restricted to clusters do not conduct K^+ in response to even excessive depolarization and that whole-cell currents were derived from the nonclustered, freely diffusing channels (O'Connell et al., 2010). A second goal was to determine whether a percentage of the endogenous Kv2.1 in cultured hippocampal neurons also exists in a nonconducting state. We report here that both transfected HEK cells and neurons typically express up to sixfold more Kv2.1 channels than measured by whole-cell voltage clamp and that nonconducting channels are present outside of cluster microdomains. Because the number of clustered and nonclustered channels is similar, up to 66% of the nonclustered channels must be nonconducting. Importantly, because the endogenous Kv2.1 channel number in cultured hippocampal neurons far exceeds the number predicted by the whole-cell ionic current, the nonconducting state is not an artifact of heterologous expression in HEK cells. It is important to keep in mind that the calculations of channel number are based on a number of assumptions and accordingly should be viewed as a best possible estimate. Detailed discussions of the assumptions and limitations are included in Materials and Methods.

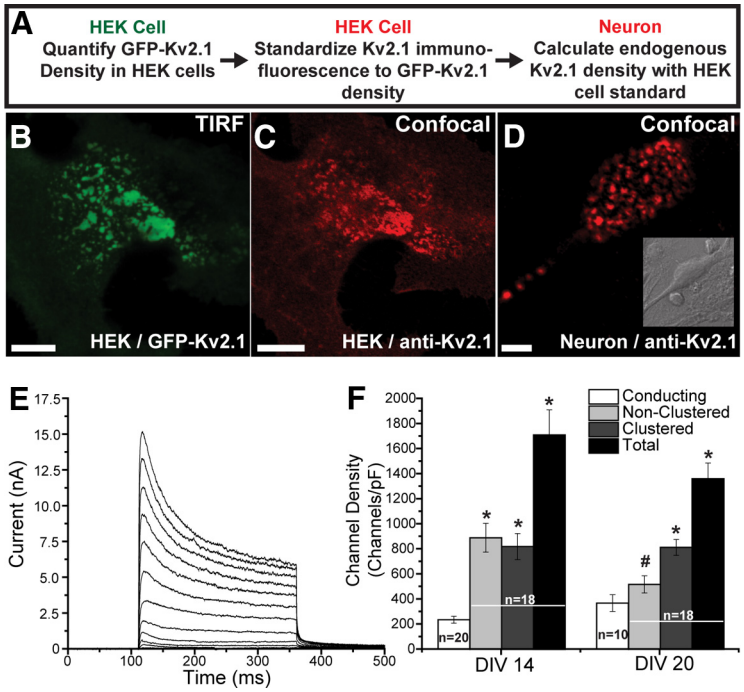

Figure 7. Calculation of endogenous Kv2.1 channel number in rat hippocampal neurons and comparison with Kv2.1 channel number estimated by voltage clamp. ***A***, A flowchart of the protocol used to measure endogenous Kv2.1 channel number in neurons. ***B***, HEK cell transfected with GFP-Kv2.1 was imaged in TIRF, and the single-channel GFP intensity was used to calculate channel density within a nonclustered region. ***C***, The same cell after fixation and immunolabeling for Kv2.1 (red) then reimaged with a confocal microscope. Antibody-derived fluorescent intensity was measured and divided by channel density determined in ***A*** to calibrate the immunostaining to Kv2.1 channel number. ***D***, DIV 14 rat hippocampal neuron immunolabeled for Kv2.1 with a DIC image inset. Endogenous Kv2.1 density of clustered, nonclustered, and total regions was calculated using transfected HEK cells (***B***, ***C***) as a standard. ***E***, Whole-cell voltage clamp recording from an embryonic day 18 rat hippocampal neuron, 14 DIV in response to 250 ms depolarizing voltage steps from +60 to −60 mV in 10 mV increments. Ik_{DR} was measured 125 ms after the depolarization to +40 mV to eliminate fast inactivating potassium currents and to avoid any Kv2.1 inactivation. ***F***, Kv2.1 channel density on DIV 14 and DIV 20 as estimated using both immunofluorescence (nonclustered, clustered, and total channel density) and whole-cell current magnitude (conducting channel density). $^*p < 0.05$, compared with conducting Kv2.1 channel density. $^{\#}p < 0.05$, compared with DIV 14. Scale bar, 10 μm.

Table 1. Endogenous Kv2.1 channel number in rat hippocampal neurons based on immunofluorescence and electrophysiology

	DIV 14	DIV 20
Current Ik_{DR} @ +40mV (pA)	10,890 ± 1,224 ($n = 20$)	16,308 ± 1,761 ($n = 10$)$^{\#}$
Conducting Kv2.1 channels	12,965 ± 1,457 ($n = 20$)	19,414 ± 2,096 ($n = 10$)$^{\#}$
Surface area (μM^2)	5,200 ± 250 ($n = 20$)	5,665 ± 714 ($n = 10$)
Clustered channels	48,313 ± 4,847 ($n = 18$)*	50,712 ± 4,122 ($n = 18$) *
Non-clustered channels	50,265 ± 6,469 ($n = 18$)*	33,059 ± 5,058 ($n = 18$)*$^{\#}$
Total channels	96,578 ± 11,317 ($n = 18$)*	85,891 ± 8,815 ($n = 18$)*
Conducting channel density (no./pF)	228 ± 27 ($n = 20$)	361 ± 67 ($n = 10$)
Clustered channel density (no./pF)	819 ± 104 ($n = 18$)*	813 ± 63. ($n = 18$)*
Nonclustered channel density (no./pF)	889 ± 114 ($n = 18$)*	519 ± 69 ($n = 18$)$^{\#}$
Total channel density (no./pF)	1709 ± 200 ($n = 18$)*	1360 ± 125 ($n = 18$)*

Kv2.1 immunofluorescence was measured in cells fixed and immunolabeled using a C-terminal Kv2.1 primary antibody (K99/14, NeuroMab) and a Alexa Fluor 594-conjugated secondary antibody (Invitrogen). Alexa Fluor 594 fluorescence was converted to channel density using immunolabeled GFP-Kv2.1 expressing HEK cells as a standard. Whole-cell electrophysiology was used to measure the delayed rectifier current, Ik_{DR}, 125 ms after step depolarizations to +40 mV. Sixty percent of the Ik_{DR} was attributed to Kv2.1, and this was converted to channel number using the single-channel conductance. Channel density was calculated by dividing channel number by the average whole-cell capacitance, C_M. Neuronal surface area was derived from whole cell capacitance ($^*p < 0.05$ compared to conducting Kv2.1; $^{\#}p < 0.05$ compared to DIV 14).

Density dependence of the nonconducting state

In HEK cells, the proportion of nonclustered channels held in the nonconducting state was strongly associated with channel membrane density. At low densities (1–20 channels/μm^2), virtually every nonclustered channel conducted K^+. As nonclustered densities increased, the fraction of nonclustered channels that were nonconducting grew steadily to 83%. Furthermore, we see the same trend with the mutant Kv2.1ΔC, which does not form classic clusters. These data strongly suggest that cluster residence itself is not the cause of the nonconducting state, but rather the high concentration of channels in this restricted space where there is a fivefold to 10-fold greater density than outside the clusters. Interestingly, a relationship between membrane density and function is not restricted to Kv2.1, for Kv1.2 and Kv3.1 channels show altered biophysical properties with increasing expression levels in *Xenopus* oocytes (Guillemare et al., 1992; Honore et al., 1992). Density-dependent function has also been reported for ligand-gated channels, such as the $P2X_2$ receptor (Fujiwara and Kubo, 2004).

Mechanism underlying the nonconducting state

The mechanism for the establishment of the nonconducting state remains unknown. Interestingly, carbon monoxide and hypoxia rapidly downregulate Kv2.1 currents without affecting the voltage dependence of activation, and these interventions could be enhancing the nonconducting population (Hulme et al., 1999; Dallas et al., 2011). The extensive regulation of Kv2.1 voltage

dependence by serine and threonine phosphorylation primarily in the carboxyl cytoplasmic termini has been well studied by Trimmer and coworkers (Park et al., 2006). More recently, Kv2.1 has been reported to be sumoylated, with sumoylation inducing a leftward shift of activation midpoint (Plant et al., 2011). Although there is no evidence that these post-translational modifications induce a nonconducting state, they are nonetheless excellent candidates, for it is easy to imagine that the proper combination of phosphorylation or dephosphorylation events could uncouple membrane depolarization and channel activation. Why does channel conductance decrease as expression density increases? Perhaps with increasing expression, a channel component or modification becomes rate-limiting at the cell surface.

The nonconducting state in HEK cells versus neurons

Whatever the mechanism inducing the nonconducting state, it appears to be, not surprisingly, more efficient in the cultured hippocampal neurons compared with HEK cells. The K^+ current density in a randomly selected population of transfected HEK cells (2144 ± 343 pA/pF, $n = 13$, data not shown) was approximately 10-fold greater than DIV 20–22 neurons (204.7 ± 22.9 pA/pF), even though the density of Kv2.1 in transfected HEK cells (497 ± 26.4 A.U./pixel, $n = 15$, data not shown) is only twofold greater than DIV 20–22 neurons (255.4 ± 36.3 A.U./pixel, $n = 11$, data not shown) based on immmunolabeling. In addition, whereas DIV 7 neurons transfected with Kv2.1 express almost threefold more channel (1217 ± 214 A.U., $n = 4$, data not shown) than transfected HEK cells, the K^+ current density is less in the transfected neurons (1377 ± 239 pA/pF, $n = 6$, data not shown) compared with HEK cells (2144 ± 343 pA/pF, $n = 13$, data not shown). This difference in the relationship between channel expression and current in HEK cells versus neurons, namely, that with similar levels of expression HEK cells produce more K^+ current, suggests that HEK cells are not as efficient as neurons with respect to induction of the nonconducting state.

Further evidence for nonconducting Kv2.1 channels

Past research has indirectly argued for a significant percentage of Kv2.1 to be playing a nonconducting role. Abundant expression of endogenous Kv2.1 is found in vascular smooth muscle where it provides a hyperpolarizing influence on the resting membrane potential (Amberg and Santana, 2006). However, although Kv2.1 is the easiest Kv channel to detect in the vasculature via Western blot analysis (Coppock and Tamkun, 2001), Kv2.1 currents in vascular smooth muscle myocytes are only 100–200 pA in magnitude (Amberg and Santana, 2006). Kv2.1 cDNA expresses well and traffics efficiently to the cell surface in heterologous expression systems and neurons as you would expect for a structural protein but not a K^+ channel. By comparison, many Kv channels are poorly delivered to the cell surface with up to 90% of the protein remaining trapped within the cell, most likely in the ER (Manganas and Trimmer, 2000). This low surface expression is understandable given that too high a membrane density will electrically silence the cell. In contrast, perhaps high levels of Kv2.1 are allowed to reach the surface considering that most of the channel will be nonconducting.

Physiological significance of the nonconducting state

Why is Kv2.1 expressed at high membrane densities where the majority of channels are nonconducting? Although it is indeed plausible that the nonconducting channels serve as a channel reservoir waiting to be activated by some stimulus, that stimulus has remained elusive (O'Connell et al., 2010). Instead, it appears that Kv2.1 has developed an accessory function, which requires an abundant supply of channel protein. Because normal neuronal function would be hindered unless there was a mechanism to silence channel conduction, the evolution of the nonconducting state was essential. Recent work by ourselves and others has demonstrated that nonconducting Kv2.1 likely plays a role in SNARE protein-based vesicular trafficking (Singer-Lahat et al., 2007; Feinshreiber et al., 2010) and that Kv2.1 clusters are sites for delivery of Kv channels, and perhaps other membrane proteins, to the cell surface (Deutsch et al., 2012). Thus, it appears that Kv2.1 has taken on functions independent of a role in controlling membrane potential. This atypical, nonchannel function likely requires a high level of expression as might be expected of a structural or scaffolding protein. Thus, the Kv2.1 nonconducting state may be a necessary property of the channel, allowing it to serve multiple functions at the cell surface without compromising electrical signaling.

References

Amberg GC, Santana LF (2006) Kv2 channels oppose myogenic constriction of rat cerebral arteries. Am J Physiol Cell Physiol 291:C348–C356. CrossRef Medline

Baver SB, O'Connell KM (2012) The C-terminus of neuronal Kv2.1 channels is required for channel localization and targeting but not for NMDA-receptor-mediated regulation of channel function. Neuroscience 217:56–66. CrossRef Medline

Coppock EA, Tamkun MM (2001) Differential expression of K(V) channel α- and β-subunits in the bovine pulmonary arterial circulation. Am J Physiol Heart Circ Physiol 281:L1350–L1360. Medline

Dallas ML, Boyle JP, Milligan CJ, Sayer R, Kerrigan TL, McKinstry C, Lu P, Mankouri J, Harris M, Scragg JL, Pearson HA, Peers C (2011) Carbon monoxide protects against oxidant-induced apoptosis via inhibition of Kv2.1. FASEB J 25:1519–1530. CrossRef Medline

Deutsch E, Weigel AV, Akin EJ, Fox P, Hansen G, Haberkorn CJ, Loftus R, Krapf D, Tamkun MM (2012) Kv2.1 cell surface clusters are insertion platforms for ion channel delivery to the plasma membrane. Mol Biol Cell 23:2917–2929. CrossRef Medline

Du J, Haak LL, Phillips-Tansey E, Russell JT, McBain CJ (2000) Frequency-dependent regulation of rat hippocampal somato-dendritic excitability by the K^+ channel subunit Kv2.1. J Physiol 522:19–31. CrossRef Medline

Feinshreiber L, Singer-Lahat D, Friedrich R, Matti U, Sheinin A, Yizhar O, Nachman R, Chikvashvili D, Rettig J, Ashery U, Lotan I (2010) Nonconducting function of the Kv2.1 channel enables it to recruit vesicles for release in neuroendocrine and nerve cells. J Cell Sci 123:1940–1947. CrossRef Medline

Fujiwara Y, Kubo Y (2004) Density-dependent changes of the pore properties of the P2X2 receptor channel. J Physiol 558:31–43. CrossRef Medline

Gentet LJ, Stuart GJ, Clements JD (2000) Direct measurement of specific membrane capacitance in neurons. Biophys J 79:314–320. CrossRef Medline

Guan D, Tkatch T, Surmeier DJ, Armstrong WE, Foehring RC (2007) Kv2 subunits underlie slowly inactivating potassium current in rat neocortical pyramidal neurons. J Physiol 581:941–960. CrossRef Medline

Guan D, Horton LR, Armstrong WE, Foehring RC (2011) Postnatal development of A-type and Kv1- and Kv2-mediated potassium channel currents in neocortical pyramidal neurons. J Neurophysiol 105:2976–2988. CrossRef Medline

Guillemare E, Honoré E, Pradier L, Lesage F, Schweitz H, Attali B, Barhanin J, Lazdunski M (1992) Effects of the level of mRNA expression on biophysical properties, sensitivity to neurotoxins, and regulation of the brain delayed-rectifier K^+ channels Kv1.2. Biochemistry 31:12463–12468. CrossRef Medline

Honoré E, Attali B, Romey G, Lesage F, Barhanin J, Lazdunski M (1992) Different types of K^+ channel current are generated by different levels of a single mRNA. EMBO J 11:2465–2471. Medline

Hulme JT, Coppock EA, Felipe A, Martens JR, Tamkun MM (1999) Oxygen sensitivity of cloned voltage-gated K^+ channels expressed in the pulmonary vasculature. Circ Res 85:489–497. CrossRef Medline

Immke D, Wood M, Kiss L, Korn SJ (1999) Potassium-dependent changes

in the conformation of the Kv2.1 potassium channel pore. J Gen Physiol 113:819–836. CrossRef Medline

Islas LD, Sigworth FJ (1999) Voltage sensitivity and gating charge in Shaker and Shab family potassium channels. J Gen Physiol 114:723–742. CrossRef Medline

Kihira Y, Hermanstyne TO, Misonou H (2010) Formation of heteromeric Kv2 channels in mammalian brain neurons. J Biol Chem 285: 15048–15055. CrossRef Medline

Kole MH, Ilschner SU, Kampa BM, Williams SR, Ruben PC, Stuart GJ (2008) Action potential generation requires a high sodium channel density in the axon initial segment. Nat Neurosci 11:178–186. CrossRef Medline

Leake MC, Chandler JH, Wadhams GH, Bai F, Berry RM, Armitage JP (2006) Stoichiometry and turnover in single, functioning membrane protein complexes. Nature 443:355–358. CrossRef Medline

Lim ST, Antonucci DE, Scannevin RH, Trimmer JS (2000) A novel targeting signal for proximal clustering of the Kv2.1 K^+ channel in hippocampal neurons. Neuron 25:385–397. CrossRef Medline

Malin SA, Nerbonne JM (2002) Delayed rectifier K^+ currents, IK, are encoded by Kv2 alpha-subunits and regulate tonic firing in mammalian sympathetic neurons. J Neurosci 22:10094–10105. Medline

Manganas LN, Trimmer JS (2000) Subunit composition determines Kv1 potassium channel surface expression. J Biol Chem 275:29685–29693. CrossRef Medline

Mashanov GI, Tacon D, Knight AE, Peckham M, Molloy JE (2003) Visualizing single molecules inside living cells using total internal reflection fluorescence microscopy. Methods 29:142–152. CrossRef Medline

Misonou H, Mohapatra DP, Park EW, Leung V, Zhen D, Misonou K, Anderson AE, Trimmer JS (2004) Regulation of ion channel localization and phosphorylation by neuronal activity. Nat Neurosci 7:711–718. CrossRef Medline

Misonou H, Mohapatra DP, Menegola M, Trimmer JS (2005) Calcium- and metabolic state-dependent modulation of the voltage-dependent Kv2.1 channel regulates neuronal excitability in response to ischemia. J Neurosci 25:11184–11193. CrossRef Medline

Misonou H, Thompson SM, Cai X (2008) Dynamic regulation of the Kv2.1 voltage-gated potassium channel during brain ischemia through neuroglial interaction. J Neurosci 28:8529–8538. CrossRef Medline

Mohapatra DP, Trimmer JS (2006) The Kv2.1 C terminus can autonomously transfer Kv2.1-like phosphorylation-dependent localization, voltage-dependent gating, and muscarinic modulation to diverse Kv channels. J Neurosci 26:685–695. CrossRef Medline

Mohapatra DP, Siino DF, Trimmer JS (2008) Interdomain cytoplasmic interactions govern the intracellular trafficking, gating, and modulation of the Kv2.1 channel. J Neurosci 28:4982–4994. CrossRef Medline

Mulholland PJ, Carpenter-Hyland EP, Hearing MC, Becker HC, Woodward JJ, Chandler LJ (2008) Glutamate transporters regulate extrasynaptic NMDA receptor modulation of Kv2.1 potassium channels. J Neurosci 28:8801–8809. CrossRef Medline

Murakoshi H, Trimmer JS (1999) Identification of the Kv2.1 K^+ channel as a major component of the delayed rectifier K^+ current in rat hippocampal neurons. J Neurosci 19:1728–1735. Medline

O'Connell KM, Tamkun MM (2005) Targeting of voltage-gated potassium channel isoforms to distinct cell surface microdomains. J Cell Sci 118: 2155–2166. CrossRef Medline

O'Connell KM, Rolig AS, Whitesell JD, Tamkun MM (2006) Kv2.1 potassium channels are retained within dynamic cell surface microdomains that are defined by a perimeter fence. J Neurosci 26:9609–9618. CrossRef Medline

O'Connell KM, Loftus R, Tamkun MM (2010) Localization-dependent activity of the Kv2.1 delayed-rectifier K^+ channel. Proc Natl Acad Sci U S A 107:12351–12356. CrossRef Medline

Pardo LA, Heinemann SH, Terlau H, Ludewig U, Lorra C, Pongs O, Stuhmer W (1992) Extracellular K^+ specifically modulates a rat brain K^+ channel. Proc Natl Acad Sci U S A 89:2466–2470. CrossRef Medline

Park KS, Mohapatra DP, Misonou H, Trimmer JS (2006) Graded regulation of the Kv2.1 potassium channel by variable phosphorylation. Science 313: 976–979. CrossRef Medline

Plant LD, Dowdell EJ, Dementieva IS, Marks JD, Goldstein SA (2011) SUMO modification of cell surface Kv2.1 potassium channels regulates the activity of rat hippocampal neurons. J Gen Physiol 137:441–454. CrossRef Medline

Scannevin RH, Murakoshi H, Rhodes KJ, Trimmer JS (1996) Identification of a cytoplasmic domain important in the polarized expression and clustering of the Kv2.1 K^+ channel. J Cell Bio 135:1619–1632. CrossRef Medline

Shaw G, Morse S, Ararat M, Graham FL (2002) Preferential transformation of human neuronal cells by human adenoviruses and the origin of HEK 293 cells. FASEB J 16:869–871. CrossRef Medline

Shi G, Kleinklaus AK, Marrion NV, Trimmer JS (1994) Properties of Kv2.1 K^+ channels expressed in transfected mammalian cells. J Biol Chem 269: 23204–23211. Medline

Singer-Lahat D, Sheinin A, Chikvashvili D, Tsuk S, Greitzer D, Friedrich R, Feinshreiber L, Ashery U, Benveniste M, Levitan ES, Lotan I (2007) K^+ channel facilitation of exocytosis by dynamic interaction with syntaxin. J Neurosci 27:1651–1658. CrossRef Medline

Stühmer W, Ruppersberg JP, Schröter KH, Sakmann B, Stocker M, Giese KP, Perschke A, Baumann A, Pongs O (1989) Molecular basis of functional diversity of voltage-gated potassium channels in mammalian brain. EMBO J 8:3235–3244. Medline

Sugiyama Y, Kawabata I, Sobue K, Okabe S (2005) Determination of absolute protein numbers in single synapses by a GFP-based calibration technique. Nat Methods 2:677–684. CrossRef Medline

Tamkun MM, O'Connell KM, Rolig AS (2007) A cytoskeletal-based perimeter fence selectively corrals a sub-population of cell surface Kv2.1 channels. J Cell Sci 120:2413–2423. CrossRef Medline

Trapani JG, Andalib P, Consiglio JF, Korn SJ (2006) Control of single channel conductance in the outer vestibule of the Kv2.1 potassium channel. J Gen Physiol 128:231–246. CrossRef Medline

Tseng-Crank J, Yao JA, Berman MF, Tseng GN (1993) Functional role of the NH2-terminal cytoplasmic domain of a mammalian A-type K^+ channel. J Gen Physiol 102:1057–1083. CrossRef Medline

Ulbrich MH, Isacoff EY (2007) Subunit counting in membrane-bound proteins. Nat Methods 4:319–321. CrossRef Medline

Weigel AV, Simon B, Tamkun MM, Krapf D (2011) Ergodic and nonergodic processes coexist in the plasma membrane as observed by single-molecule tracking. Proc Natl Acad Sci U S A 108:6438–6443. CrossRef Medline

Yang J, Thio LL, Clifford DB, Zorumski CF (1993) Electrophysiological properties of identified postnatal rat hippocampal pyramidal neurons in primary culture. Brain Res Dev Brain Res 71:19–26. CrossRef Medline